

Alunogen from the sulfate efflorescence of the Stone Town Nature Reserve in Ciężkowice (the Outer Carpathian Mountains, Poland)

Mariola Marszałek¹, Adam Gaweł²

¹AGH University of Krakow, Faculty of Geology, Geophysics and Environmental Protection, Krakow, Poland, e-mail: mmarszal@agh.edu.pl, ORCID ID: 0000-0001-6062-0322

²AGH University of Krakow, Faculty of Geology, Geophysics and Environmental Protection, Krakow, Poland; e-mail: agaweł@agh.edu.pl, ORCID ID: 0000-0002-3158-2045

© 2023 Author(s). This is an open access publication, which can be used, distributed and re-produced in any medium according to the Creative Commons CC-BY 4.0 License requiring that the original work has been properly cited.

Received: 4 November 2022; accepted: 19 May 2023; first published online: 7 June 2023

Abstract: Alunogen ($\text{Al}_2(\text{SO}_4)_3 \cdot 17\text{H}_2\text{O}$), a rare secondary mineral, has been found in the efflorescence on sandstones from the Stone Town Nature Reserve in Ciężkowice, southeastern Poland. This is probably the first find of this salt on such rocks in Poland. Alunogen forms in various geological environments, but mainly from the oxidation of pyrite and other metal sulfides in ore deposits and Al-rich Earth materials under low-pH conditions. Its crystallization at this particular site depends on a set of necessary physicochemical (pH, concentration), climatic (season, temperature, humidity), site-related (location and protection of efflorescence), and mineralogical (the presence of pyrite) conditions. This paper presents the mineralogical and geochemical characteristics of the alunogen from the Stone Town Nature Reserve (based on SEM-EDS, XRPD, EPMA and Raman spectroscopy methods) as well as of the efflorescence itself (based on XRPD and STA coupled with QMS and FTIR for the analysis of gas products). Crystals of alunogen take the shape of flakes, often with a hexagonal outline, clustered in aggregates forming a cellular network. Its calculated formula is $(\text{Al}_{1.96}\text{Fe}_{0.01}^{3+})_{\Sigma 1.97}(\text{SO}_4)_3 \cdot 17\text{H}_2\text{O}$ (based on 12 O and 17 H_2O). The unit-cell parameters refined for the triclinic space group $P\bar{1}$ are: $a = 7.423$ (1) Å, $b = 26.913$ (5) Å, $c = 6.056$ (1) Å, $\alpha = 89.974$ (23)°, $\beta = 97.560$ (25)°, $\gamma = 91.910$ (22)°. The Raman spectra (SO_4) bands are: intensive 995 cm^{-1} (ν_1); low-intensive 1069 , 1093 and 1127 cm^{-1} (ν_3); low-intensive 419 and 443 ; medium-intensive 470 cm^{-1} (ν_2); and medium-intensive 616 cm^{-1} (ν_4). Those at 530 , 312 and at 338 cm^{-1} are assigned to water vibrations and those at 135 , 156 , 180 cm^{-1} to the lattice modes. Although the efflorescence contained an admixture of other minerals (pickeringite, gypsum and quartz), the predominant alunogen is almost chemically pure and the above parameters are consistent with the values reported in the literature for alunogen from different locations and of various origins.

Keywords: sulfate efflorescence, alunogen, thermal analysis, Raman spectroscopy, unit-cell parameters, the Carpathian Mountains, Poland

INTRODUCTION

Alunogen is a naturally occurring hydrous aluminum sulfate that crystallizes in the triclinic space group $P\bar{1}$, but a low-temperature modification (monoclinic space group $P2_1$) is also known (Kahlenberg et al. 2015). This mineral is most often chemically described as a heptadecahydrate with

the chemical formula $\text{Al}_2(\text{SO}_4)_3 \cdot 17\text{H}_2\text{O}$. Depending on the position of the water molecules, the formula can also be written as $\text{Al}_2(\text{SO}_4)_3(\text{H}_2\text{O})_{12} \cdot 5\text{H}_2\text{O}$.

The crystallographic structure of alunogen consists of sheets of isolated $\text{Al}(\text{Ow})_6$ octahedra and SO_4 tetrahedra which are linked by a network of hydrogen bonds. Twelve structural H_2O (among 17 per alunogen formula) are coordinated

with Al and behave as ligands, where oxygen is bound to Al atoms and acts as a proton donor for the sulfate oxygens. The remaining five structural H₂O exist in the interstitial spaces parallel to [001] between tetrahedra and octahedra. This water is usually referred to as “free” or “zeolitic” and is responsible for the slightly variable composition of alunogen when the mineral is in contact with air of low humidity. The crystallographic structure of alunogen is given in Figure 1. The maximum water content of alunogen is 17 molecules (Fang & Robinson 1976), and the lower number of H₂O molecules per formula unit, reported by some authors, is explained by partial dehydration, resulting from the partial release of “free” water from the crystal structure. As a consequence, the real amount of water is less, probably between 16 and 17 water molecules per formula unit (Menchetti & Sabelli 1974, Fang & Robinson 1976, Kahlenberg et al. 2015, 2017). However, at relative humidities below 20%, at room temperature, the formation of so-called meta-alunogen has been observed, which only contains about 13.7 water molecules pfu (Kahlenberg et al. 2017).

Alunogen has been found in a variety of geological settings. Its origin is associated mainly with oxidation of pyrite or other metal sulfides in ore deposits in aluminum-rich environments, leading to the alteration of aluminosilicate minerals under low pH conditions (Alpers et al. 1994, Hammarstrom et al. 2005, Joeckel et al. 2005). The occurrence of alunogen also requires specific atmospheric conditions. It has been found to be sensitive to ambient humidity and temperature, and these change with the seasons (Fang & Robinson 1976, Marszałek et al. 2020). Furthermore, being a highly soluble salt (Hammarstrom & Smith 2002), in moderately humid climates alunogen can only survive in areas protected from the rain, such as in rock niches or beneath overhangs (Williams & Robinson 1998, Alexandrowicz & Marszałek 2019).

Alunogen is frequently found in association with other sulfates, such as epsomite MgSO₄·7H₂O, pickeringite MgAl₂(SO₄)₄·22H₂O, halotrichite FeAl₂(SO₄)₄·22H₂O, gypsum CaSO₄·2H₂O, melanterite Fe²⁺(H₂O)₆SO₄·H₂O (FeSO₄·7H₂O), coquimbite AlFe₃(SO₄)₆(H₂O)₁₂·6H₂O, copiapite (Fe²⁺, Mg)

Fe³⁺(SO₄)₆(OH)₂·20H₂O, alunite KAl₃(SO₄)₂(OH)₆ and potassium alum KAl(SO₄)₂·12H₂O (Williams & Robinson 1998, Jambor et al. 2000, Hammarstrom & Smith 2002, Joeckel et al. 2005, Frost et al. 2007, Příkryl et al. 2007, Varilowa et al. 2011, Naglik et al. 2016a, Gomes et al. 2017, Košek et al. 2018, Alexandrowicz & Marszałek 2019, Marszałek et al. 2020, Szabo et al. 2020).

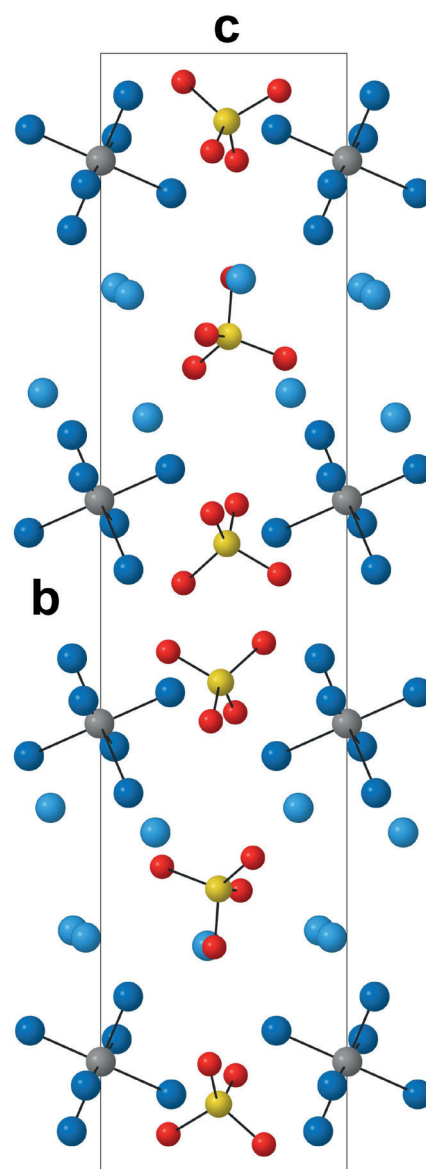


Fig. 1. Crystal structure of alunogen. Explanations: red and dark blue spheres represent oxygen atoms of the sulfate groups and of water molecules coordinated to the aluminum atoms, respectively; light blue, yellow and gray spheres: “free” water, sulfur and aluminum atoms positions, respectively; b, c – unit-cell edges

Over 260 different alunogen sites are listed in the mindat.org database (<http://www.mindat.org>, accessed July 13, 2022). This mineral is often found in sulfide-bearing ore mines, particularly abandoned ones, in waste dumps of such deposits and tailing dumps (Wieser 1949, Parafiniuk 1996, Jambor et al. 2000, Hammarstrom et al. 2005, Gomes et al. 2017, Biagioni et al. 2020). The mineral has been discovered in coal mines and self-burning dumps of coal mine waste (Žáček 1988, Parafiniuk & Stępisiewicz 1999, Stracher et al. 2005, Kruszewski 2013, 2019, Žáček & Skála 2015). In addition, alunogen has been observed as a product of the alteration of various rocks under the influence of acidic sulfate fluids, e.g., in volcanic fumarole incrustations (Hall et al. 2003, Adams et al. 2017, Rodríguez & van Bergen 2017, Luo et al. 2019, Garavelli et al. 2021), as a component of crusts in caves containing H₂S thermal springs (Audra & Hobléa 2007) and also as an alteration product of kaolinite in ignimbrites (Martin et al. 1999). Alunogen has been found to be a phase occurring in the efflorescences on weathered argillaceous rocks that contain pyrite (Williams & Robinson 1998, Naglik et al. 2015). Alunogen has also been reported in efflorescences on sandstones (Williams & Robinson 1998, Vařilová et al. 2011, Alexandrowicz & Marszałek 2019). Lastly, alunogen has been also reported as a result of the weathering of microscopic pyrite veins in metamorphic, quartz-feldspar rocks due to the contact with meteoric water (Szabo et al. 2020). Alunogen has also been suggested to be a part of the Al-bearing deposits on Mars (Wang & Zhou 2014, Kahlenberg et al. 2017, Košek et al. 2018, 2022).

Alunogen has been found in a few locations in Poland, including pyrite-bearing sericite-chlorite schists in Wieściszowice, Lower Silesia (Balcerzak et al. 1992, Parafiniuk 1996), the Shale Formation in the Pieprzowe Mountains (Naglik & Natkaniec-Nowak 2015, Naglik et al. 2016a, 2016b), an iron disulfide deposit of the Holy Cross Mountains (Wieser 1949); in spontaneously combusting coal-mine waste dumps in the Upper and Lower Silesian Coal Basins (Parafiniuk & Stępisiewicz 1999, Kruszewski 2013, Ciesielczuk et al. 2014), and on the sandstone tor from the Stone Town Nature Reserve in Ciężkowice in the Outer

Carpathian Mountains (Alexandrowicz & Marszałek 2019).

Alunogen efflorescences on the sandstone tor from the Stone Town Nature Reserve (STNR) in Ciężkowice (the Polish Outer Carpathian Mountains), is found with other Al-sulfate such as pickeringite (calculated formula $Mg_{0.75}Mn_{0.21}Zn_{0.02}Cu_{0.01}Al_{2.02}(S_{0.99 \text{ to } 1.00}O_4)_4 \cdot 22H_2O$) and gypsum (Alexandrowicz & Marszałek 2019, Marszałek et al. 2020). Marszałek et al. (2020) have already characterized pickeringite from the study site and discussed the genesis of aluminum-rich efflorescences there. This paper characterizes alunogen, another Al-sulfate found on the Ciężkowice STNR tor. To the best of the authors' knowledge, this is the first detailed characterization of alunogen occurring on sandstones in Poland. Characterization of the alunogen-containing efflorescence was performed using X-ray powder diffraction (XRPD) and simultaneous thermal analysis (STA) coupled with quadrupole mass spectrometry (QMS) and Fourier Transform Infrared spectroscopy (FTIR) for the analysis of gas products. The combination of XRPD and STA coupled with QMS and FTIR techniques allows a more comprehensive analysis of the samples, especially in the case of samples containing amorphous phases. The detailed mineralogical and geochemical characterization of alunogen was performed based on scanning electron microscopy combined with energy dispersive spectrometry (SEM-EDS), electron microprobe analysis (EPMA) and Raman microspectroscopy (RS). The XRPD patterns collected for the complete samples of the efflorescence were used to refine the unit-cell parameters of alunogen.

GEOLOGICAL SITE

The STNR in the village of Ciężkowice (49°46'36"N, 20°57'50"E) (the Ciężkowice Foothills, Outer Flysch Carpathian Mountains) is known for its picturesque landforms with numerous freestanding sandstone tors, partly hidden in a pine forest (Fig. 2). The rocks in the area represent the Upper Paleocene to Lower Eocene Ciężkowice Sandstone Formation of the Silesian Nappe. This site was extensively studied by Alexandrowicz (1970, 1978, 1987, 2008), and Alexandrowicz & Marszałek (2019).

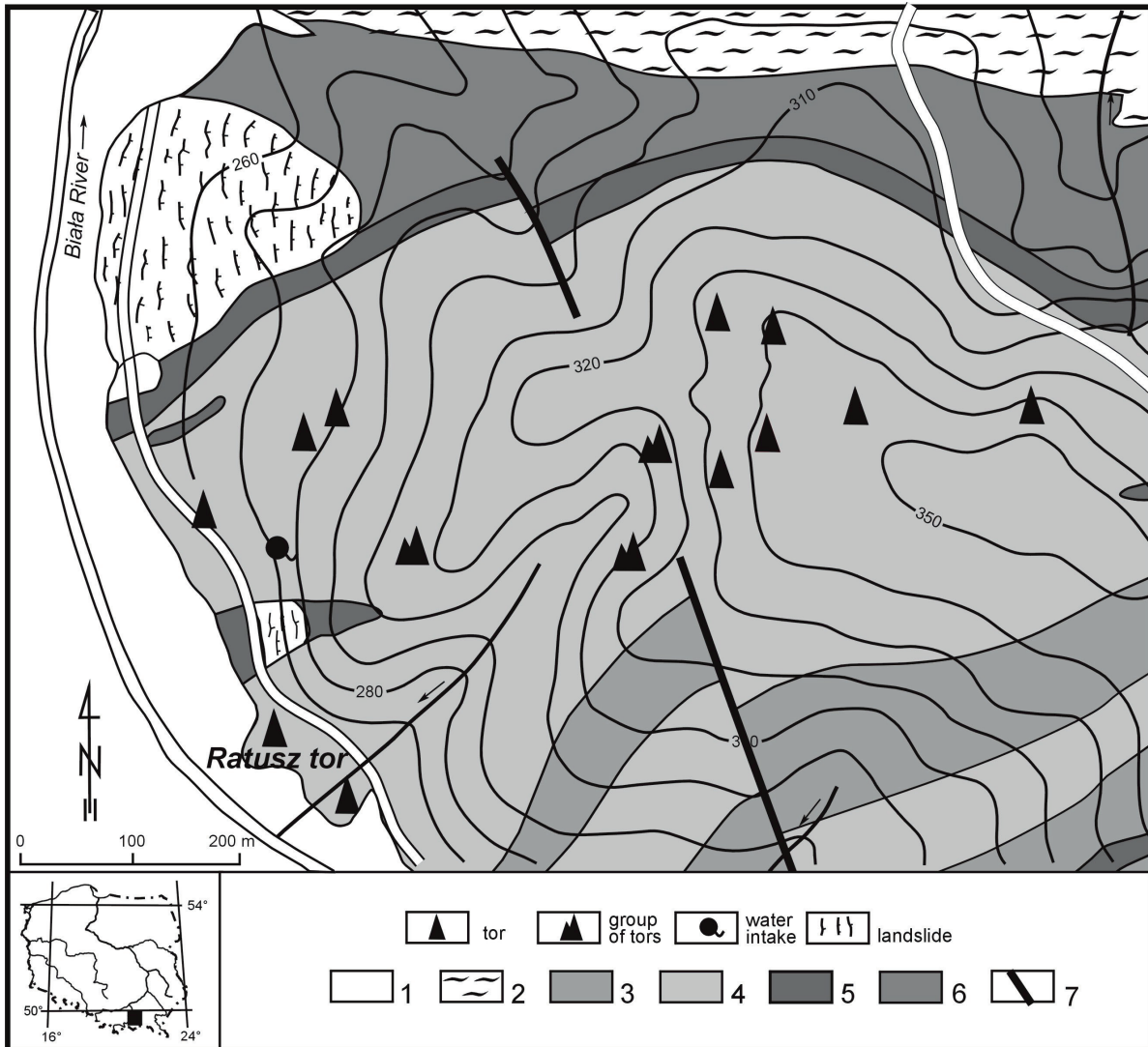


Fig. 2. Geological map and distribution of the sandstone tors of the Stone Town Nature Reserve (STNR), Ciężkowice area (after Alexandrowicz 1970, Leszczyński 1981, Cieszkowski et al. 1991, modified). Quaternary deposits: 1 – alluvial clays; 2 – alluvial and diluvial loams. Paleogene flysch sequences: 3 – Hieroglyphic Beds (green shales and sandstones); 4 – Ciężkowice Sandstones (conglomeratic sandstones, sandstones, conglomerates); 5 – Variegated and Red Shales (shales); 6 – Upper Istebna Shales (shales); 7 – fault

The Ciężkowice sandstones are mostly represented by quartz arenites and wackes, occasionally subarcose or feldspathic wackes (Leszczyński 1981, Leszczyński et al. 2015) with a cement of a mixed porous-contact nature. The wacke matrix consists of kaolinite and illite with admixtures of interstratified illite-smectite group minerals. Cement phases are carbonates, dark patches are pigmented by iron (oxyhydr)oxides. A common accessory phase is pyrite, often altered to goethite (Alexandrowicz & Marszałek 2019). In some places, the stony tor surfaces are coated with a crust chiefly containing the Fe minerals hematite and

goethite (Alexandrowicz et al. 2014). Ca-, Mg-, K-, and Al-sulfates, including gypsum, syngenite, hexahydrate, pentahydrate, potassium-alum, humberstonite, alunogen and pickeringite exist in efflorescences on many of the sandstone tors (Alexandrowicz & Marszałek 2019). The mineral composition of the efflorescences differ depending on the location of the tor. Most of the tors are on hillslopes that rise as much as 100 m above local stream valleys. There are also single tors on the valley bottom of the Biała River, just above its flood terrace (Fig. 2) (Alexandrowicz & Marszałek 2019, Marszałek et al. 2020).

MATERIALS AND METHODS

Alunogen-rich efflorescence was encountered in a niche protected from rain on the Ratusz (“Town Hall”) tor (Figs. 2, 3). Within the STNR, it was only here that Al-rich sulfates were found. Their formation within the Ratusz tor is influenced by a number of factors. Alunogen has crystallized at the study site because of the availability of weatherable pyrite, low environmental pH, moderate atmospheric humidity and summer season, as well as the location of the tor in the valley bottom directly above the floodplain of the Biała River and sheltered microenvironment. These conditions have already been characterized in the works of Alexandrowicz & Marszałek (2019) and Marszałek et al. (2020).

The efflorescences are whitish (10YR 8/1) (Munsell Color 1998), brittle, botryoidal clusters of very fine granules. Pure alunogen could not be mechanically isolated from other microscopic crystals in the multiphase efflorescences, although individual crystals of the mineral were readily identified with electron microscopy.

Laboratory investigations focused on the analyses of complete samples of the efflorescences or on the alunogen crystals only, depending on the methods applied.

The X-ray diffractometry (XRPD) studies for powdered samples of the efflorescence were carried out using a Rigaku SmartLab 9 kW diffracto-

meter, equipped with a reflective graphite monochromator. Cu-K α radiation was used. The diffraction data were collected within the angular range of 3–72° 2 θ with the step of 0.02°, and a counting time of 2 s per step at a voltage of 45 kV, and a current of 200 mA. Quartz from Jegłowa, Poland, was used as an internal standard. The XRPD patterns were evaluated by an XRAYAN software using a diffraction pattern database of International Centre for Diffraction Data (ICDD) (The Powder Diffraction File PDF-4+, 2016). Diffraction peak positions were determined automatically using the derivatives method as a procedure of the XRAYAN software.

The alunogen unit-cell parameters were refined for the triclinic space group $P\bar{1}$ in accordance with the data of the ICDD database (entry no. 26-1010). The least-squares method and the DHN-PDS (DHN-Powder Diffraction System version 2.3, 1994) program were applied. The calculation was based on twenty-five reflections of alunogen that did not overlap with reflections of other components of the efflorescence.

Simultaneous thermal analyses (including thermogravimetry, differential thermal analysis, differential thermogravimetry – TG, DTA, DTG) of the efflorescence was conducted in a STA 449 F3 Jupiter Netzsch instrument coupled to a QMS 403 C Aëolos mass spectrometer and FTIR Bruker Tensor 27 spectrometer allowing the determination of gaseous decomposition products.

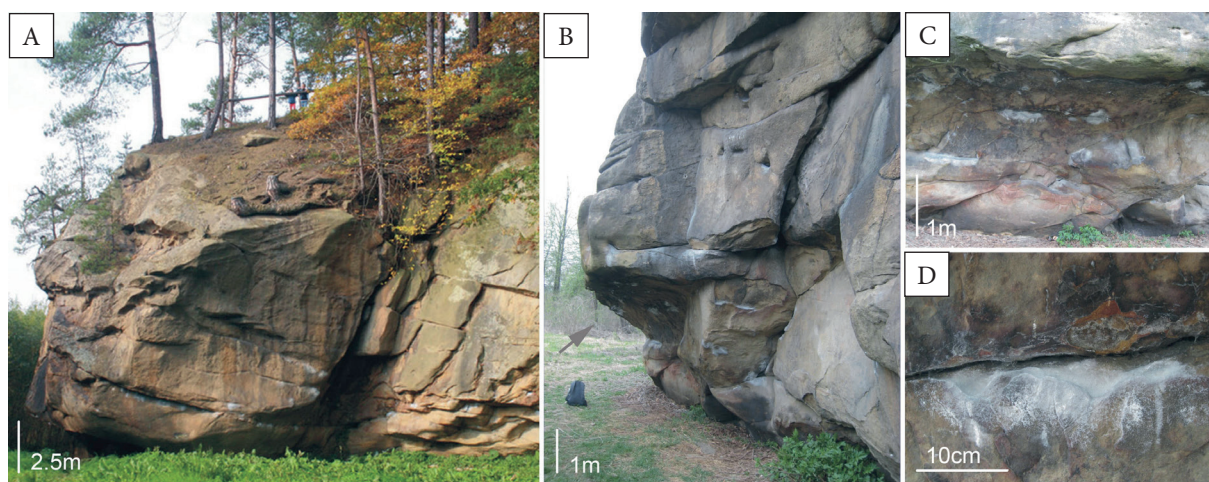


Fig. 3. The Ratusz (“Town Hall”) tor in the STNR (A) (for location see Fig. 2), and the niche with a whitish alunogen efflorescence (B, C, D)

The data obtained by QMS reveals differently ionized molecules and their fragments and cannot resolve compounds with the same m/z values, while FTIR detects only those substances that change dipoles. A powdered sample of the efflorescence with a weight of about 30 mg was heated in the air (flow was set to 40 cm³/min) in the range 20–1000°C with a constant heating rate of 10°C/min. Al₂O₃ powder was used as the thermally inert substance.

Alunogen from the efflorescence was analyzed using a FEI 200 Quanta FEG scanning electron microscope equipped with an EDS/EDAX spectrometer. Observations were carried out in the low vacuum mode (pressure of 60 Pa, the samples were not coated) at a maximum excitation voltage of 20 kV.

Quantitative chemical analyses (EPMA) were performed using a JEOL Super Probe JXA-8230 operating in the wavelength dispersion (WDXS) mode. The operating conditions were: an accelerating voltage of 15 kV, a beam current of 1 nA, a beam size of 7–10 μm, a peak count time of 20 s, and background time of 10 s. Standards, analytical lines, diffracting crystals, and mean detection limits (in wt%) were as follows: fluorapatite (PKα, PET, 0.27), (CaKα, PET, 0.04), albite (NaKα, TAP, 0.14), (SiKα, TAP, 0.12) and (AlKα, TAP, 0.11), diopside (MgKα, TAP, 0.09), sanidine (KKα, PET, 0.03), anhydrite (SKα, PET, 0.11), rhodonite (MnKα, LIF, 0.33), fayalite (FeKα, LIF, 0.28), barite (BaLα, PET, 0.25), celestine (SrLα, PET, 0.26), cuprite (CuKα, LIF, 0.14), and willemite (ZnKα, LIF, 0.22). The raw data were corrected using the ZAF procedure. The atomic contents of the formulae of alunogen were calculated on the basis of 12 oxygen atoms per formula unit (apfu) with the assumed presence of 17 water molecules pfu. The analyses were conducted on carbon-coated fragments of the efflorescence embedded in 1 inch resin discs and polished using oil.

Raman spectra of alunogen were collected using a Thermo Scientific DXR Raman microscope with a 900 grooves/mm grating and a CCD detector. Excitation was provided by a 532 nm laser with a maximum power of 10 mW. To obtain spectra of the best quality 10–100 scans were taken, each with a 3 s exposure time. For the same reason, the laser power varied in the range of 3–10 mW. Olympus 10× (NA 0.25) and 50× (NA 0.50) objectives

(theoretical spot sizes 2.1 μm and 1.1 μm, respectively) were employed. The spectra were analyzed based on the RRUFF Raman Minerals spectral libraries as well as some data from literature (Košek et al. 2018, 2022). Band component identification was performed using the Omnic software package (Omnic 9, 1992–2012, Thermo Fisher Scientific Inc.). Band fitting was conducted using a Gauss–Lorentz cross product function (for the fitting process, the minimum number of component bands were used).

RESULTS AND DISCUSSION

Efflorescence from the Ratusz tor

X-ray powder diffractometry (XRPD)

The powder X-ray diffraction patterns of the efflorescence sample showed the dominance of alunogen with an admixture of pickeringite and gypsum. Additionally, traces of quartz were also found in the sample (Fig. 4A). The phases were identified based on the following data: alunogen, ICDD database entry no. 26-1010, pickeringite, ICDD database entry no. 46-1454 and from Quartieri et al. (2000), gypsum, ICDD entry no. 33-311 and quartz ICDD entry no. 33-1161.

STA, mass spectrometry QMS and FTIR spectroscopy analyses

The STA (DTA, TG and DTG) curves of the efflorescence are shown in Figure 5. FTIR-3D (absorbance as a function of wavenumber and temperature) of the evolved gaseous decomposition products released under heating of the sample in air is presented in Figure 6. The FTIR spectra of the gaseous decomposition products, extracted from all collected spectra from FTIR-3D at five temperatures corresponding to the temperatures of maximal DTG effects are presented in Figure 7. Temperature-dependent ion current (IC) and changes in the absorbance of selected range wavenumbers (FTIR temperature trace) extracted from FTIR-3D are shown in Figure 8. The first set shows the IC of the differently ionized molecule and its fragments, while the second shows the changes in absorbance of selected wavenumber ranges.

Five major thermal decomposition steps are noted (Fig. 5).

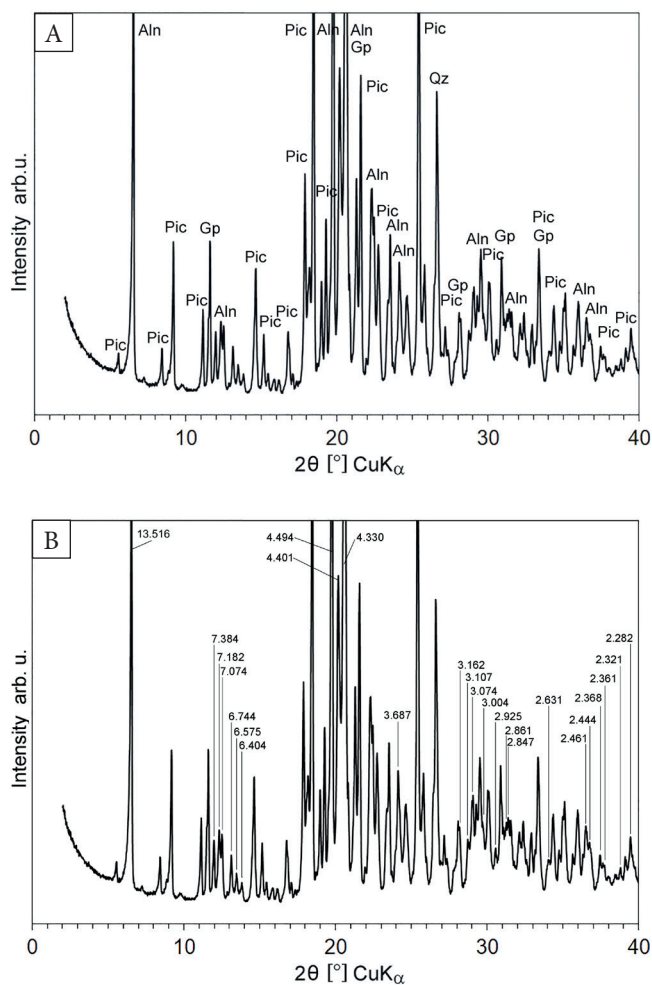


Fig. 4. Characteristic X-ray patterns of the Al-rich efflorescence from the Ratusz tor (A) and the alunogen reflections used for the refining unit-cell parameters (B). Abbreviations: Aln – alunogen; Gp – gypsum; Pic – pickeringite; Qz – quartz

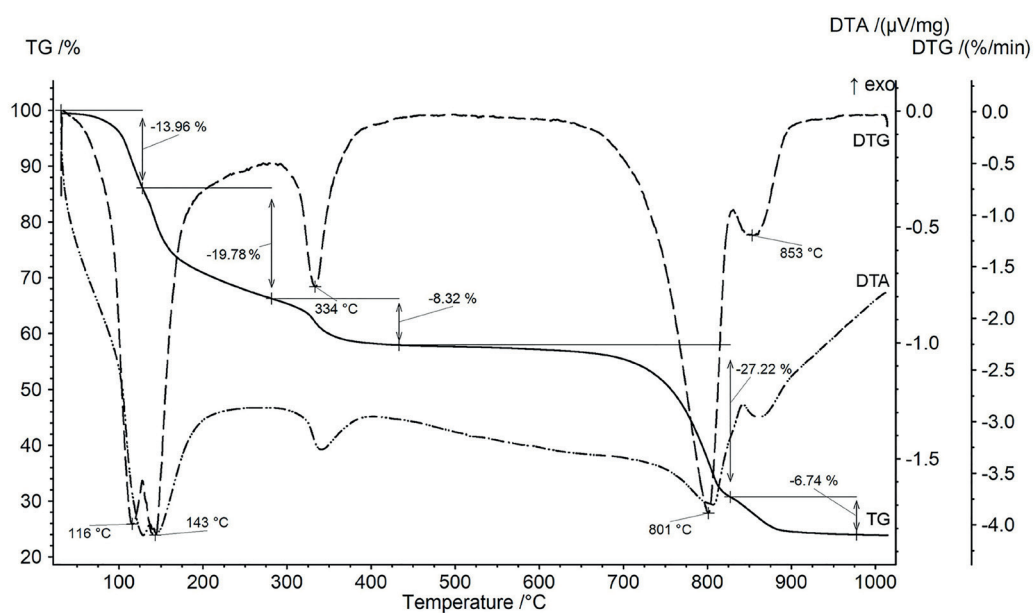


Fig. 5. STA (DTA, TG and DTG) curves for the efflorescence samples from the Ratusz tor (STNR)

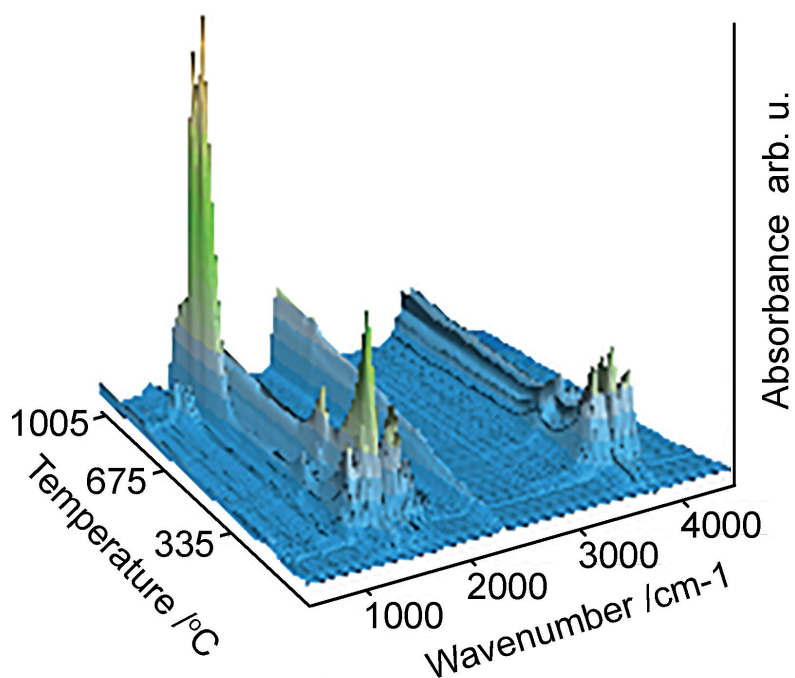


Fig. 6. FTIR-3D (wavenumber- and temperature-dependent FTIR absorbance) of the evolved gaseous decomposition products formed upon heating of the efflorescence samples from the Ratusz tor (STNR) in air

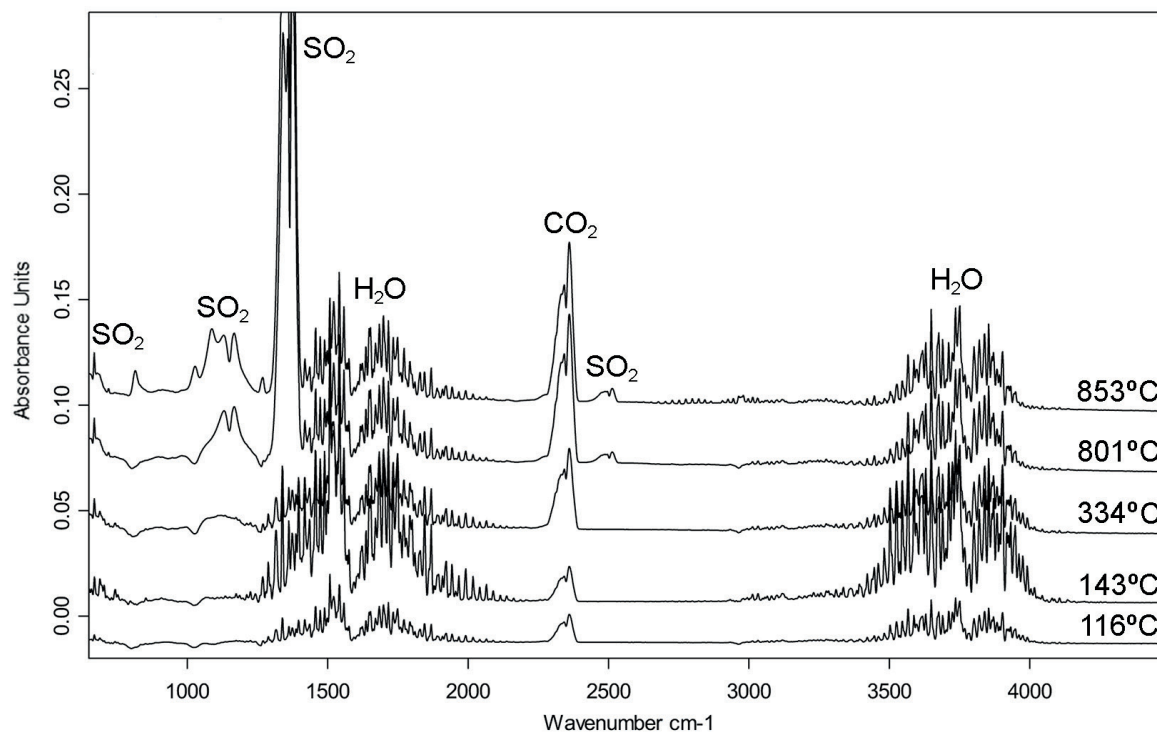


Fig. 7. FTIR spectra of the gaseous decomposition products emitted upon heating by the efflorescence sample from the Ratusz tor (STNR) in the presence of air. The spectra were selected from all the spectra collected during the analysis (FTIR-3D) and correspond to the maximum temperature of each of the five mass loss effects (DTG curve)

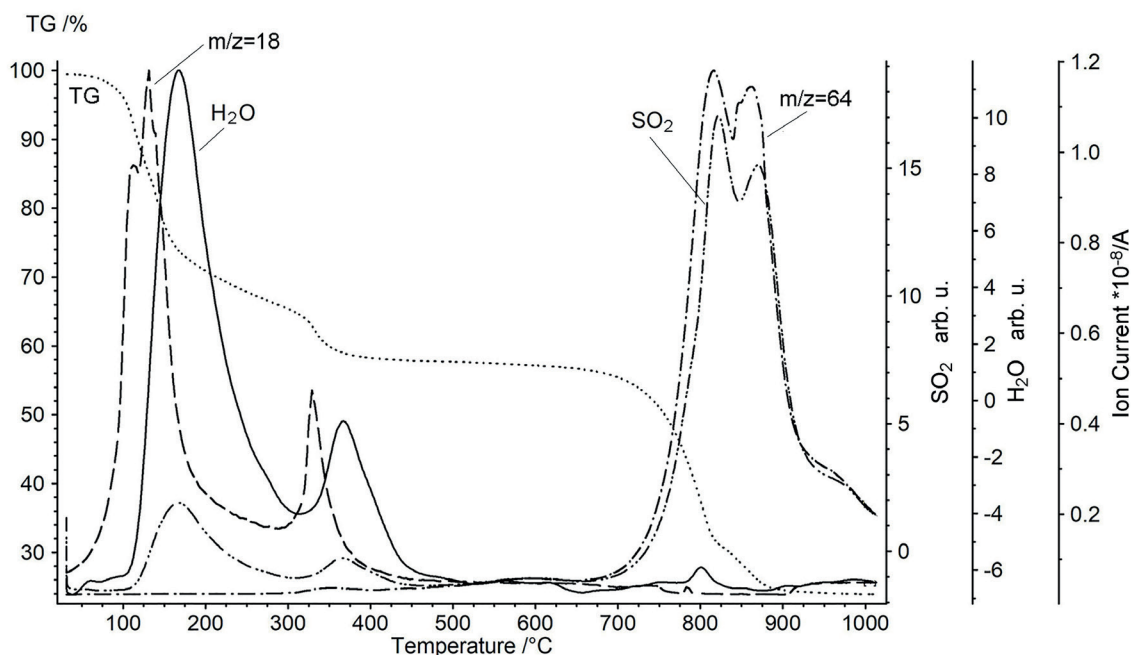


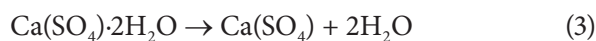
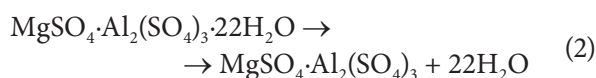
Fig. 8. Temperature-dependent ion current (IC) and changes in the absorbance of a selected range of wavenumbers extracted from FTIR-3D curves of the volatile decomposition products formed upon heating of the efflorescence samples from the Ratusztor (STNR) in air. Ion current curves for $m/z = 18$ (H_2O) and $m/z = 64$ (SO_2) and FTIR temperature-dependent curves of SO_2 ($1035\text{--}1260\text{ cm}^{-1}$) and H_2O ($3400\text{--}4000\text{ cm}^{-1}$) are presented in relation to the TG curve. (The observed shifts of maxima in the QMS and FTIR temperature-dependent curves are caused by the axial temperature gradient in the measurement chamber and the influence of the bandwidth of the transfer line of the furnace chamber on the FTIR and QMS analyzer)

In the low temperature region, two effects (1st and 2nd step) at 116°C and 143°C are observed. The mass losses are 13.96% and 19.78% respectively ($\Sigma 33.74\%$). The next (3rd) step occurs at 334°C and results in a mass loss of 8.32%. These three effects are attributed to the gradual loss of water from the hydrated minerals in the sample, and are confirmed by the current signal curves at $m/z = 18$ indicating the presence of H_2O (Fig. 8). The QMS curve shows a maxima at 112°C , 132°C and 329°C . The third endothermic effect is related to the complete dehydration of the minerals. The water molecules that are lost at this much higher temperature are strongly bound to the minerals (most probably trapped in their structure). The total mass loss due to dehydration is 42.06%.

The FTIR-3D revealed significant changes in the intensities of particular absorption bands of the decomposition products as a function of temperature (Fig. 6). On the spectra, extracted from all the collected spectra for the temperatures attributed with loss of water (116 , 143 , 334°C ; DTA, TG curves), the presence of the characteristic

absorption bands of H_2O are mainly observed (Fig. 7). The bands in the ranges $1230\text{--}2100\text{ cm}^{-1}$ and $3400\text{--}4000\text{ cm}^{-1}$ confirmed the emission of water vapor from the sample (Chukanov & Chervonnyi 2016). The low intensity band in the range $2260\text{--}2400\text{ cm}^{-1}$ with a maximum at 2350 cm^{-1} is attributed to CO_2 . However, the band indicating the presence of carbon dioxide is not associated with the sample components (using all of the methods employed, no carbonate minerals were found in the samples) and may arise due to the presence of atmospheric CO_2 in the infrared beam path between the source and detector (Chukanov & Chervonnyi 2016). The FTIR temperature trace curve for H_2O (to avoid coincidence with the bands of SO_2 , the range between $3400\text{--}4000\text{ cm}^{-1}$ was chosen) shows good agreement with the IC curve for $m/z = 18$ (Fig. 8). The observed shifts of the curves' maxima are due to the axial temperature gradient in the measurement chamber and the influence of the bandwidth of the transfer line of the furnace chamber with the FTIR and QMS analyzer.

For steps 1, 2 and 3 the following reactions are proposed:



The next steps (4 and 5) are observed at the temperatures of 801°C and 853°C. The mass losses in these steps are 27.22% and 6.74%, resulting in a total mass loss of 33.96% (Fig. 5). The observed decomposition involves the formation of metal oxides and the release of SO₃, followed by the decomposition of SO₃ into SO₂ and O₂. Corresponding ionic current peaks with maxima at 816°C and 861°C at $m/z = 64$ (SO₂) are observed (Fig. 8).

FTIR spectra characteristic for these steps (Fig. 7) reveal the bands at the ranges 1035–1260 cm⁻¹ with a maximum at *ca.* 1156 cm⁻¹ and 1290–1450 cm⁻¹ with a maximum at 1363 cm⁻¹ and are related to ν_1 and ν_3 vibrations of SO₂ respectively (Buzykin et al. 2005). A low intensity band at *ca.* 2500 cm⁻¹ is also related to sulfur dioxide (Rothman et al. 1992, Buzykin et al. 2005). The other observed bands are much less intense and may be related to atmospheric H₂O and CO₂ (gas atmosphere inside the furnace; Chukanov & Chervonnyi 2016). The bands characteristic for SO₃ (Buzykin et al. 2005) have not been observed. The FTIR temperature-dependent curve for SO₂ (the range between 1035–1260 cm⁻¹ was selected as characteristic for SO₂) shows good agreement with the IC curve for $m/z = 64$ (Fig. 8). The range characteristic for the ν_1 vibration of SO₂ slightly overlaps with that for water (1230–2100 cm⁻¹), hence the FTIR temperature trace curve for SO₂ shows an elevation of the line in the range indicating the presence of water (see FTIR temperature trace curve of H₂O).

XRPD analysis of the final thermal decomposition product of the efflorescence sample (carried out after the measurement was completed) shows the presence of spinel MgAl₂O₄ (ICDD database entry no. 21-1152), anhydrite CaSO₄ (ICDD database entry no. 37-1496) and quartz (ICDD entry no. 33-1161). This indicates that, at least for the applied measurement parameter settings, both anhydrous aluminum sulfates decomposed with the release of SO₃ followed by the decomposition of

SO₃ into SO₂ and O₂. The endothermic effects occurring at the temperatures of 801°C and 853°C are associated with the decomposition of aluminum and magnesium sulphates respectively. Thermal decomposition of CaSO₄ occurs at a higher temperature (*ca.* 1200°C; Földvári 2011), and was therefore not recorded. The lack of an endothermic reaction (DTA curve) at 573°C, indicative of a structural transformation of β quartz (low-temperature quartz) into α quartz (high-temperature quartz), is evidence that there were only minor amounts of the phase in the sample.

The following decomposition is generally proposed:



The total mass loss from the decomposition of the sample attributed to the water loss steps is 42.06%, which is lower than the theoretical mass loss of 47.23% in alunogen. However, this seems to be a reasonable outcome given the presence of admixtures such as pickeringite and gypsum, affecting these values. In addition, the total mass loss attributed to the SO₃ release steps is lower than the theoretical mass loss (33.96% and 37.04% respectively). However, it is important to note that the effect of decomposition at the temperature of 801°C with a mass loss of 27.22% is related to the decomposition of aluminum sulfate coming from both alunogen and pickeringite, while the next step, at the temperature of 853°C with a mass loss of 6.47%, is linked to the decomposition of magnesium sulfate from pickeringite. The total mass loss attributed to the SO₃ release steps do not include the gas released from dehydrated gypsum, that is anhydrite (CaSO₄ decomposes at temperatures above 1000°C).

Comparing the results obtained with those available in the literature, some difficulties and discrepancies are encountered. The key point is that natural samples of efflorescence are usually a mixture of salt minerals, resulting in complex thermal effects (Frost et al. 2007, Locke et al. 2007). Isomorphic substitutions in minerals also affect

the observed thermal effects, such as minerals in the halotrichite mineral group (Locke et al. 2007, Földvári 2011). This also results in a lack of corresponding literature data. In the sample from the Ratusz tor, both the thermal effects associated with the dehydration of the sulfate minerals and the decomposition of the anhydrous sulfates – alunogen and pickeringite occur in a very similar temperature range (Földvári 2011), and cannot be attributed separately to individual salts. It is most likely that only the effect at 853°C can be solely attributed to the decomposition of MgSO_4 from pickeringite. Therefore, the amounts of specific sulfate minerals in the sample, based on their characteristic mass losses, cannot be clearly quantified. Our analysis of the recorded thermal effects generally agrees with published data regarding the sulfate minerals present in the sample, particularly alunogen.

Kahlenberg et al. (2017) indicate that the discrepancies in the characterization of alunogen samples by different researchers result from the degree of crystallinity of the sample, the two to five steps in the release of structural water (Gancy et al. 1981), and the setting of STA measurement parameters. The latter include well-known parameters affecting thermal effects e.g. amount of material, heating rates, water vapor pressure or gas atmosphere (air, nitrogen, argon and vacuum) inside the furnace. However, irrespective of these factors, the end product of the dehydration of alunogen is anhydrous $\text{Al}_2(\text{SO}_4)_3$. Finally, aluminum sulfate decomposes into metal oxide with

the release of SO_3 followed by the decomposition of SO_3 into SO_2 and O_2 . The final thermal decomposition products of the Ratusz tor efflorescence (MgAl_2O_4 , CaSO_4 and SiO_2) reflect the complex composition of the sample and the reactions occurring between the metal oxides formed after the release of SO_3 from dehydrated alunogen and pickeringite, under the conditions in which the measurements were carried out.

Alunogen from Stone Town Nature Reserve

SEM-EDS analysis

Alunogen crystals were found to be the main component of the whitish botryoidal aggregates of salt efflorescence from the Ratusz tor. In the SEM microscopic images, it forms flaky crystals, frequently exhibiting a hexagonal outline. The crystals range from a few dozen to a hundred μm in size. They are clustered in aggregates which coalesce to form a cellular network (Fig. 9A, B). Based on EDS analysis, only Al, S and O were found in its chemical composition. The other components of the efflorescence are pickeringite and gypsum. Pickeringite, of the chemical formula $(\text{Mg}_{0.75}\text{Mn}_{0.21}\text{Zn}_{0.02}\text{Cu}_{0.01})(\text{S}_{0.99\text{ to }1.00}\text{O}_4) \cdot \text{Al}_{2.02}(\text{S}_{0.99\text{ to }1.00}\text{O}_4)_3 \cdot 22\text{H}_2\text{O}$ (Marszałek et al. 2020), forms aggregates of very fine and thin acicular crystals, not exceeding several hundred micrometers in length. Gypsum is the rarest phase exhibiting a prismatic shape, showing the presence of Ca, S and O in EDS analysis.

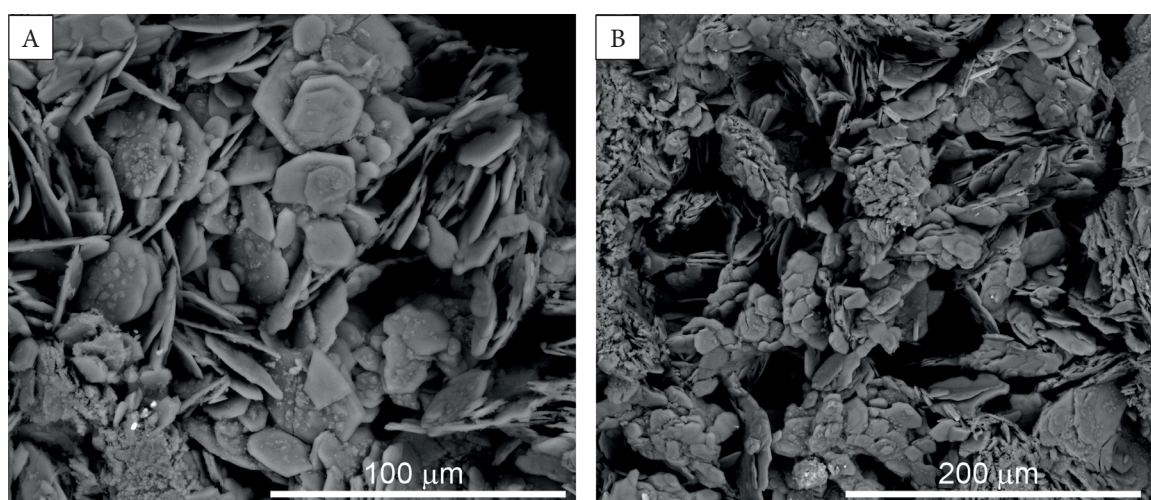


Fig. 9. Back scattered electron (BSE) images of alunogen from the Ratusz tor efflorescence (A, B)

Chemical analysis (EPMA)

The microprobe analyses are presented in Table 1.

Table 1

Representative chemical compositions of the STNR alunogen

Chemical compositions	Analysis number					Average <i>n</i> = 5	sd
	2	6	9	10	11		
[wt%]							
SO ₃	35.84	37.25	37.04	35.67	36.15	36.39	0.71
P ₂ O ₅	0.00	0.00	0.06	0.16	0.00	0.04	0.07
SiO ₂	0.00	0.00	0.03	0.05	0.00	0.02	0.02
Al ₂ O ₃	15.36	15.24	15.12	15.69	14.87	15.26	0.30
CuO	0.00	0.00	0.00	0.07	0.00	0.01	0.03
ZnO	0.10	0.00	0.09	0.03	0.22	0.09	0.08
SrO	0.00	0.00	0.00	0.06	0.00	0.01	0.03
MnO	0.00	0.12	0.04	0.00	0.45	0.12	0.19
FeO	0.31	0.00	0.03	0.21	0.07	0.12	0.13
CaO	0.00	0.04	0.01	0.04	0.04	0.03	0.02
BaO	0.30	0.00	0.00	0.00	0.24	0.11	0.15
MgO	0.09	0.17	0.17	0.48	0.17	0.22	0.15
Na ₂ O	0.21	0.01	0.08	0.13	0.21	0.13	0.09
K ₂ O	0.00	0.03	0.01	0.02	0.05	0.02	0.02
H ₂ O*	46.20	47.24	47.04	46.58	46.26	46.67	0.46
Total	98.42	100.10	99.74	99.19	98.71	99.23	0.70
[apfu]**							
S ⁶⁺	2.97	3.02	3.01	2.93	2.99	2.98	0.04
P ⁵⁺	0.00	0.00	0.01	0.01	0.00	0.00	0.01
Σ	2.97	3.02	3.02	2.94	2.99	2.98	0.03
Si ⁴⁺	0.00	0.00	0.00	0.01	0.00	0.00	0.00
Al ³⁺	2.00	1.94	1.93	2.02	1.93	1.96	0.04
Cu ²⁺	0.00	0.00	0.00	0.01	0.00	0.00	0.00
Zn ²⁺	0.01	0.00	0.01	0.00	0.02	0.01	0.01
Sr ²⁺	0.00	0.00	0.00	0.00	0.00	0.00	0.00
Mn ²⁺	0.00	0.01	0.00	0.00	0.04	0.01	0.02
Fe ²⁺	0.03	0.00	0.00	0.02	0.01	0.01	0.01
Ca ²⁺	0.00	0.00	0.00	0.00	0.00	0.00	0.00
Ba ²⁺	0.01	0.00	0.00	0.00	0.01	0.00	0.01
Mg ²⁺	0.02	0.03	0.03	0.08	0.03	0.04	0.02
Na ⁺	0.05	0.00	0.02	0.03	0.04	0.03	0.02
K ⁺	0.00	0.00	0.00	0.00	0.01	0.00	0.00
Total	5.09	5.00	5.01	5.11	5.08	5.05	0.05
H ₂ O	17	17	17	17	17	17	

sd – standard deviation,

* calculated from stoichiometry,

** calculated on the basis of 12 O atoms per formula unit (apfu) with the presence of 17 H₂O molecules pfu.

In this study, Fe was calculated as FeO. Since the concentration of this element is very low, converting it to Fe₂O₃ does not significantly change the analytical results and does not influence the calculated chemical formula. The concentration of

FeO varies from 0.00 to 0.31 wt% (0.12 wt% ±0.13 and 0.01 apfu ±0.01 on average). Alunogen from STNR contains 14.87–15.69 wt% (15.26 wt% on average) of Al₂O₃ and 35.84–37.25 wt% (36.39 wt% on average) of SO₃. Elements, such as Mn, Zn and Cu, occur in traces (0.12 wt%, 0.09 wt% and 0.01 wt% respectively, giving ≤0.01 apfu on average) and are likely related to the co-occurrence of pickeringite. Alkali and alkaline earth metals: Na (Na₂O 0.13 wt% on average), K (K₂O 0.02 wt% on average), Ba (BaO 0.11 wt% on average), Mg (MgO 0.22 wt% on average) and Ca (CaO 0.03 wt% on average) probably come from neighboring minerals (e.g., gypsum and pickeringite) and/or thin clay material from the efflorescence. Silica (SiO₂), that was present in the studied material in the amount of 0.03–0.05 wt%, should be considered as finely dispersed quartz. Its presence was also confirmed by XRPD analyses. Based on the results obtained (FeO converted to Fe₂O₃), the possible empirical formula of alunogen from STNR is: (Al_{1.93 to 2.02}Fe³⁺_{0.00 to 0.03})_{Σ1.93 to 2.05}(S_{0.98 to 1.01}O₄)₃·17H₂O (ideal water content assumed). The final proposed empirical formula, based on the average results, is: (Al_{1.96}Fe³⁺_{0.01})_{Σ1.97}(SO₄)₃·17H₂O. It seems that the deficiency or the excess of sulfur and cations is most likely to be caused by an admixture of alunogen with other minerals in the analyzed volume, and possibly also by the instability of hydrous minerals under an electron beam.

Unit-cell parameters

The calculation of unit-cell parameters was carried out on the basis of twenty-five reflections of alunogen that do not overlap with the reflections of other components of the efflorescence (Fig. 4A, B). The unit-cell parameters, refined for the triclinic space group *P* $\bar{1}$, are as follows: *a* = 7.423 (1) Å, *b* = 26.913 (5) Å, *c* = 6.056 (1) Å, α = 89.974 (23)°, β = 97.560 (25)°, γ = 91.910 (22)°. Although the samples contained an admixture of other sulfates (pickeringite and gypsum), the predominant alunogen was relatively chemically pure ((Al_{1.96}Fe³⁺_{0.01})_{Σ1.97}(SO₄)₃·17H₂O). Trace amounts of additional cations in some crystals (not exceeding 0.04 apfu on average) do not seem to influence the unit-cell parameters. The results obtained are consistent with data previously reported for this mineral by other researchers (Fig. 10).

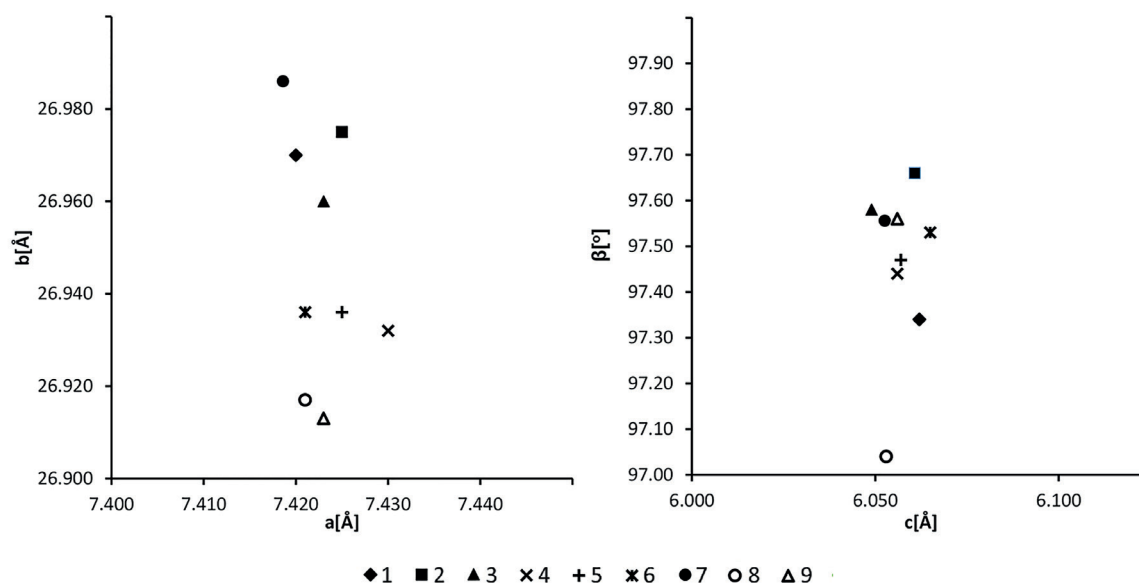


Fig. 10. Unit-cell parameters of the STNR alunogen compared to data in the literature: 1 – Fang & Robinson (1976); 2 – Menchetti & Sabelli (1974); 3 – Žáček (1988); 4, 5 – Košek et al. (2018); 6 – Kruszewski (2013); 7 – Biagioni et al. (2020); 8 – Szabo et al. (2020); 9 – this paper

Raman microspectroscopy

The Raman spectrum of alunogen is divided into three regions (Košek et al. 2018): the first from 900 to 1300 cm^{-1} , dominated by the spectral signatures of the SO_4 stretching vibrations; the second region below 800 cm^{-1} , containing the spectral signatures of the SO_4 bending vibrations as well as lattice and water vibrations; the third segment from 3000 to 3600 cm^{-1} , containing the stretching vibrations of the hydroxyl groups.

The spectrum in the region of 900–1300 cm^{-1} (Fig. 11) display the strong band at 995 cm^{-1} assigned to the ν_1 (SO_4) symmetric stretching vibration. The next low-intensity bands in this region are assigned to the asymmetric stretching mode ν_3 (SO_4) and can be found at 1069, 1093 and 1129 cm^{-1} . The region below 800 cm^{-1} contains a weak band at 419, and a broad one composed of two bands at 443 and 473 cm^{-1} , representing the symmetric bending ν_2 vibration of the sulfate tetrahedra.

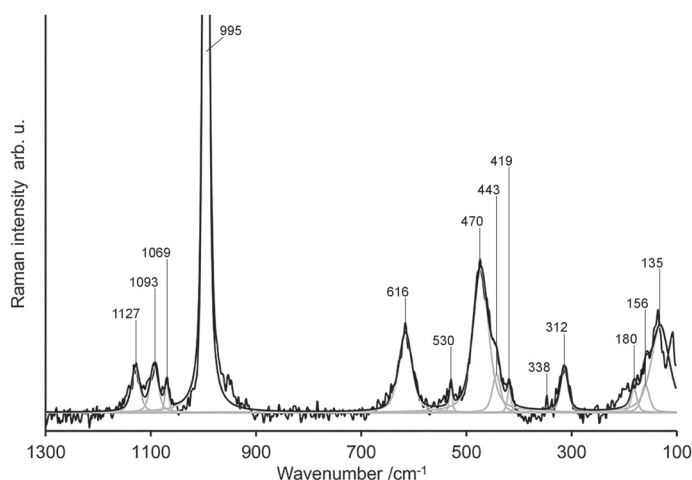


Fig. 11. Raman spectra of the STNR alunogen in the 100–1300 cm^{-1} region

Low intensity bands at 530, 314 and a very weak band at 338 cm^{-1} can be assigned to water vibrations. The first one, at 530 cm^{-1} , could also be attributed to the ν_2 (SO_4) vibration. A broad band at 614 cm^{-1} of medium intensity can be assigned to the asymmetric bending ν_4 vibration. Lattice vibrational modes were registered in the lower wavenumber regions at 132, 160, 181 cm^{-1} . The bands characteristic of the OH-stretching vibration, in the region between 3000 and 3600 cm^{-1} , were not recorded. However, the presence of water in the crystal structure of alunogen is marked by bands of water vibrations at 314, 338 and 530 cm^{-1} .

The Raman bands of alunogen from the Ratusztor correspond closely to data published by other researchers (Table 2).

The position of the strongest Raman band assigned to the ν_1 (SO_4) symmetric stretching vibration (995 cm^{-1}) differs only slightly from that reported by Wang & Zhou (2014), Košek et al. (2018, 2022) and Szabo et al. (2020) (992 cm^{-1}) and is almost identical to data given by Buzatu et al. (2016) (996 cm^{-1}). This observation confirms the relatively regular position of the ν_1 (SO_4) vibration in alunogen samples from different locations and origins. The same logic applies to other vibration modes, with the exception of OH-stretching vibrations, which did not appear in the spectrum. Their presence is reported however by Wang & Zhou (2014), Košek et al. (2018) and Szabo et al. (2020), but not in Buzatu et al. (2016).

Table 2

The Raman bands with their assignments for alunogen (natural and synthetic samples)

Wang & Zhou 2014	Buzatu et al. 2016	Košek et al. 2018		Košek et al. 2022	Szabo et al. 2020	This study	Assignment (follows Košek et al. 2018)	
(1)	(2)	(3)	(4)	(5)	(6)	(7)		
		138 w		136 m		132	135	lattice mode
		155 w	156 w	154 vw			156	lattice mode
		180 w	182 w	184vw		219	180	lattice mode
				278 vw				lattice mode
309	316	310 w	310 w	308 w	307	305	312	water vibration
		338 vw	344 vw	340 vw	341		338	water vibration
	427	415 vw	414 sh	415 vw	418		419	ν_2 (SO_4)
		445 sh	445 w				443	ν_2 (SO_4)
470	473	470 m	473 m	469 m	469	463	470	ν_2 (SO_4)
		528 vw	528 w	528 vw	529		530	water vibration or ν_2 (SO_4)
612	608	614 m	611 m	612 m	613	612	616	ν_4 (SO_4)
			642 w					ν_4 (SO_4)
	849							
992	996	992 vs	992 vs	992 vs	992	992	995	ν_1 (SO_4)
		1066 w	1069 sh	1066 w	1067		1069	ν_3 (SO_4)
1086	1080	1089 w	1086 m	1088 w	1085	1083	1093	ν_3 (SO_4)
1126		1127 m	1127 m	1126 m	1123	1144	1127	ν_3 (SO_4)
3246		~3160 br	~3220 br	~3240 br		~3267		(OH) stretch vibration
		~3351 br		~3440 br		~3406		(OH) stretch vibration

Samples origin/source: (1) synthetic, pure, crystalline, declared formula $\text{Al}_2(\text{SO}_4)_3 \cdot 17\text{H}_2\text{O}$, ACROS; (2) abandoned Minei Hill open pit, Baia Sprie mining area, Romania; (3) Schoeller coal mine, Kladno, Czech Republic, empirical formula $(\text{Al}_{1.99}\text{Fe}_{0.01}^{3+})(\text{SO}_4)_3 \cdot 17\text{H}_2\text{O}$; (4) synthetic, Penta Prague, Czech Republic, declared formula $\text{Al}_2(\text{SO}_4)_3 \cdot 16\text{H}_2\text{O}$; (5) burning coal waste dump, Alsdorf, Germany; (6) Jiul de Vest Upper Basin, South Carpathian Mountains, Romania; (7) STNR, Ciężkowice, Outer Carpathian Mountains, Poland, empirical formula $\text{Al}_{1.96}\text{Fe}_{0.01}^{3+}\text{Fe}_{0.01}^{2+}(\text{SO}_4)_3 \cdot 17\text{H}_2\text{O}$.

The symbols 's', 'm', 'w', 'v', 'sh' and 'br' used next to the position of the Raman bands refer to their intensities: strong, medium, weak, very, shoulder and broad respectively.

At the same time, variation in the case of the hydroxyl bands (especially spectral intensity) has been reported in the literature (Wang & Zhou 2014). This specific broad band of the OH vibration is explained by a very high number of water molecules occupying various, structurally independent sites in the alunogen structure. Twelve structural H₂O molecules (out of 17 per alunogen formula) are coordinated with the two Al cations, 6 per cation (Fig. 1), which results in different bond lengths between H₂O and Al in these two types of octahedra. This produces an extremely broad spectra band centered around 3250 cm⁻¹ in the Raman spectrum. Further broadening of the H₂O band in the vibrational spectrum is associated with the remaining five structural H₂O molecules not coordinated to the Al cations. These are bounded to the alunogen structure through weak hydrogen bonds and are located in the interstitial spaces between the SO₄ tetrahedra and Al(H₂O)₆ octahedra. This location results in differences in the symmetry of the bonds. Partial dehydration of alunogen (partial loss of hydrogen bonded water), which can lead to a higher degree of structural ordering, i.e. better defined crystallographic sites for structural water, is reflected in the variable intensity and shape of hydroxyl bands (i.e. new bands may appear) (Wang & Zhou 2014).

SUMMARY AND CONCLUDING REMARKS

This paper presents the mineralogical and geochemical characteristics of natural alunogen which is a component of the efflorescence on a sandstone tor in STNR in Poland, along with a characterization of the efflorescence itself.

Phase analysis (XRPD) of the efflorescence revealed the dominance of alunogen with an admixture of other sulfate salts – pickeringite and traces of gypsum. Thermal analysis coupled with evolved gas mass spectrometry QMS and FTIR spectroscopy showed that the efflorescence samples revealed thermal decomposition steps at 116, 143 and 334°C, which are attributed to the gradual loss of water from the hydrated minerals in the sample (adsorbed water, interstitial water and chemically bonded water). The efflorescence sample also

showed two higher temperature decomposition steps at 801 and 853°C, related to the decomposition of anhydrous sulfates, with the release of SO₃, followed by the decomposition of SO₃ into SO₂ and O₂. The effect of decomposition at the temperature 801°C is related to the decomposition of aluminum sulfate from both alunogen and pickeringite, while the next, at 853°C, is linked solely to the decomposition of magnesium sulfate from pickeringite. The total measured mass loss (concerning the effects attributed to alunogen) is lower than the theoretical mass loss in alunogen. This difference may be explained by a number of factors: the sample analyzed contains admixtures of other sulfates, the mineral studied is a natural mineral, and finally, the mass loss of adsorbed water is not taken into account in the total measured mass loss (i.e. the total measured mass loss also includes the loss of adsorbed water). Despite the fact that the sample was a mixture of minerals, the analysis of the recorded thermal effects generally agrees with the published data regarding the sulfate minerals present in the sample, particularly alunogen.

Alunogen crystals, the dominant component of the Ratusz tor efflorescence, is almost chemically pure, and its calculated empirical formula is (Al_{1.96}Fe_{0.01})_{Σ1.97}(SO₄)₃·17H₂O. Deviation from the ideal stoichiometry is most likely to be caused by an admixture of alunogen with other minerals in the analyzed volume, and possibly also by the instability of hydrous minerals under an electron beam. The refined unit cell parameters of the investigated specimens are consistent with the values reported in the literature for alunogen of various origins and are as follows: $a = 7.423$ (1) Å, $b = 26.913$ (5) Å, $c = 6.056$ (1) Å, $\alpha = 89.974$ (23)°, $\beta = 97.560$ (25)°, $\gamma = 91.910$ (22)°, giving a ratio $a:b:c = 0.275:1:0.225$. The Raman spectra of this Al-rich sulfate from the Ratusz tor is in close agreement with data published by other researchers. The characteristic bands are registered at 995 cm⁻¹ (ν_1 SO₄); 1069, 1093 and 1129 cm⁻¹ (ν_3 SO₄); 419, 443 and 473 cm⁻¹ (ν_2 SO₄), and 614 cm⁻¹ (ν_4 SO₄). Bands at 530, 314 and at 338 cm⁻¹ are assigned to water vibrations. Lattice vibrational modes were registered at 132, 160, 181 cm⁻¹. The bands characteristic for the OH-stretching vibration, in the region between 3000 and 3600 cm⁻¹, were not recorded.

Characterization of the alunogen containing efflorescence performed using both X-ray powder diffraction (XRPD) and simultaneous thermal analysis (STA) coupled with quadrupole mass spectrometry (QMS) and Fourier Transform Infrared spectroscopy (FTIR) for the analysis of gas products is one of the first studies of this type. Using STA alongside XRPD gives more complete information about efflorescent minerals. Taking into account the fact that studies of aluminum sulfates are quite rare in the literature, the results obtained could be valuable reference data for the characteristics of other various geological materials containing such sulfates.

The studies were supported by the AGH University of Krakow, grant number 16.16.140.315.

The authors acknowledge the help of Adam Włodek for performing EPMA measurements. We also thank the three anonymous reviewers for their helpful comments towards improving the original manuscript.

REFERENCES

- Adams P.M., Lynch D.K., Buckland K.N., Johnson P.D. & Tratt D.M., 2017. Sulfate mineralogy of fumaroles in the Salton Sea Geothermal Field, Imperial County, California. *Journal of Volcanology and Geothermal Research*, 347, 15–43. <https://doi.org/10.1016/j.jvolgeores.2017.08.010>.
- Alexandrowicz Z., 1970. Skałki piaskowcowe w okolicy Ciężkowic nad Białą [Sandstone rocks in the vicinity of Ciężkowice on the Biała River]. *Ochrona Przyrody*, 35, 281–335.
- Alexandrowicz Z., 1978. Skałki piaskowcowe zachodnich Karpat fliszowych [Sandstone tors of the Western Flysch Carpathians]. *Prace Geologiczne – Polska Akademia Nauk. Oddział w Krakowie. Komisja Nauk Geologicznych*, 113, Zakład Narodowy im. Ossolińskich – Wydawnictwo PAN, Wrocław.
- Alexandrowicz Z., 1987. Przyroda nieożywiona Czarnorzecznego Parku Krajobrazowego [Inanimate nature in the Czarnorzeczek Landscape Park]. *Ochrona Przyrody*, 45, 263–293.
- Alexandrowicz Z., 2008. Sandstone rocky forms in Polish Carpathians attractive for education and tourism. *Przeгляд Geologiczny*, 56(8/1), 680–687.
- Alexandrowicz Z. & Marszałek M., 2019. Efflorescences on weathered sandstone tors in the Stone Town Nature Reserve in Ciężkowice the Outer Carpathians, Poland – their geochemical and geomorphological controls. *Environmental Science and Pollution Research*, 26(36), 37254–37274. <https://doi.org/10.1007/s11356-019-06778-4>.
- Alexandrowicz Z., Marszałek M. & Rzepa G., 2014. Distribution of secondary minerals in crusts developed on sandstone exposures. *Earth Surface Processes & Landforms*, 39(3), 320–335. <https://doi.org/10.1002/esp.3449>.
- Alpers C.N., Blowes D.W., Nordstrom D.K. & Jambor J.L., 1994. Secondary minerals and acid mine-water chemistry. [in:] Jambor J. & Blowes D. (eds.), *The Environmental Geochemistry of Sulfide Mine-wastes: Short Course Handbook*, Mineralogical Association of Canada, Waterloo, ON, Canada, 247–270.
- Audra P. & Hobléa F., 2007. The first cave occurrence of jurbanite $[\text{Al}(\text{OH SO}_4)_2 \cdot 5\text{H}_2\text{O}]$, associated with alunogen $[\text{Al}_2(\text{SO}_4)_3 \cdot 17\text{H}_2\text{O}]$ and tschermigite $[\text{NH}_4\text{Al}(\text{SO}_4)_2 \cdot 12\text{H}_2\text{O}]$: thermal-sulfidic Serpents Cave, France. *Journal of Cave and Karst Studies*, 69(2), 243–249.
- Balcerzak E., Dobrzyński D. & Parafiniuk J., 1992. Wpływ przeobrażeń mineralnych na skład chemiczny wód w strefie wietrzenia łupków pirytonośnych w Wieściszowicach. *Annales Societatis Geologorum Poloniae*, 62, 75–93.
- Biagioni C., Mauro D. & Pasero M., 2020. Sulfates from the pyrite ore deposits of the Apuan Alps (Tuscany, Italy): A review. *Minerals*, 10(12), 1092. <https://doi.org/10.3390/min10121092>.
- Buzatu A., Dill G.H., Buzgar N., Damian G., Maftai A.E. & Apopei A.I., 2016. Efflorescent sulfates from Baia Sprie mining area (Romania) – Acid mine drainage and climatological approach. *Science of the Total Environment*, 542(Part A), 629–641. <https://doi.org/10.1016/j.scitotenv.2015.10.139>.
- Buzykin O.G., Ivanov S.V., Ionin A.A., Kotkov A.A., & Kozlov A.Y., 2005. Spectroscopic detection of sulfur oxides in the aircraft wake. *Journal of Russian Laser Research*, 26(5), 402–426. <https://doi.org/10.1007/s10946-005-0043-z>.
- Chukanov N.V. & Chervonnyi A.D., 2016. *Infrared Spectroscopy of Minerals and Related Compounds*. Springer Mineralogy, Springer Cham.
- Ciesielczuk J., Kruszewski Ł., Fabiańska M.J., Misz-Kennan M., Kowalski A. & Mysza B., 2014. Efflorescences and gas composition emitted from the burning coal-waste dump in Słupiec, Lower Silesian Coal Basin, Poland. [in:] Macek I. (ed.), *Proceedings of the International Symposium CEMC 2014, Skalský Dvůr, Czech Republic, 23–26 April 2014*, 26–27.
- Cieszkowski M., Koszarski A., Leszczyński S., Michalik M., Radomski A. & Szulc J., 1991. *Szczegółowa mapa geologiczna Polski 1:50 000. Arkusz Ciężkowice*. Wydawnictwa Geologiczne, Warszawa.
- Fang J.H. & Robinson P.D., 1976. Alunogen, $\text{Al}_2(\text{H}_2\text{O})_{12}(\text{SO}_4)_3 \cdot 5\text{H}_2\text{O}$: its atomic arrangement and water content. *American Mineralogist*, 61(3–4), 311–317.
- Földvári M., 2011. *Handbook of Thermogravimetric System of Minerals and Its Use in Geological Practice*. Occasional Papers of the Geological Institute of Hungary, 213, Budapest, Hungary.
- Frost R.L., Wain D., Martens W.N., Locke A.C., Martinez-Frias J. & Rull F., 2007. Thermal decomposition and X-ray diffraction of sulphate efflorescent minerals from El Jaroso Ravine, Sierra Almagrera, Spain. *Thermochimica Acta*, 460(1–2), 9–14. <https://doi.org/10.1016/j.tca.2007.05.011>.

- Gancy A.B., Rao J.M. & Wenner W.M., 1981. Dehydration behaviour of aluminium sulfate hydrates. *Journal of the American Ceramic Society*, 64(2), 119–123. <https://doi.org/10.1111/j.1151-2916.1981.tb09588.x>.
- Garavelli A., Pinto D., Mitolo D. & Kolitsch U., 2021. Thermesaite-(NH₄), (NH₄)₂AlF₃(SO₄), a new fumarole mineral from La Fossa crater at Vulcano, Aeolian Islands, Italy. *Mineralogical Magazine*, 85(5), 665–672. <https://doi.org/10.1180/mgm.2021.69>.
- Gomes P., Valente T. Grande J.A. & Cordeiro M., 2017. Occurrence of sulphate efflorescences in São Domingos mine. *Comunicações Geológicas*, 104(1), 83–89.
- Hall A.J., Fallick A.E., Perdikatsis V. & Photos-Jones E., 2003. A model for the origin of Al-rich efflorescences near fumaroles, Melos, Greece: enhanced weathering in a geothermal setting. *Mineralogical Magazine*, 67(2), 363–379. <https://doi.org/10.1180/0026461036720102>.
- Hammarstrom J.M. & Smith K.S., 2002. Geochemical and mineralogical characterization of solids and their effects on waters in metal-mining environments. [in:] Seal R.R. II & Foley N.K. (eds.), *Progress on Geo-environmental Models for Selected Mineral Deposit Types*, US Geological Survey Open-File Report 02-195, US Geological Survey, Reston, VA, USA, 8–54.
- Hammarstrom J.M., Seal R.R. II, Meier A.L. & Kornfeld J.M., 2005. Secondary sulfate minerals associated with acid drainage in the eastern US: Recycling of metals and acidity in surficial environments. *Chemical Geology*, 215(1–4), 407–431. <https://doi.org/10.1016/j.chemgeo.2004.06.053>.
- Jambor J.L., Nordstrom D.K. & Alpers C.N., 2000. Metal-sulfate salts from sulfide mineral oxidation. *Reviews in Mineralogy & Geochemistry*, 40(1), 303–350. <https://doi.org/10.2138/rmg.2000.40.6>.
- Joeckel R.M., Ang Clement B.J & VanFleet Bates L.R., 2005. Sulfate mineral crusts, pyrite weathering, and acid rock drainage in the Dakota Formation and Graneros Shale (Cretaceous), Jefferson County, Nebraska. *Chemical Geology*, 215(1–4), 433–452. <https://doi.org/10.1016/j.chemgeo.2004.06.044>.
- Kahlenberg V., Braun D.E. & Orlova M., 2015. Investigations on alunogen under Mars relevant temperature conditions: an example for a single-crystal-to-single-crystal phase transition. *American Mineralogist*, 100(11–12), 2548–2559. <https://doi.org/10.2138/am-2015-5342>.
- Kahlenberg V., Braun D.E., Krüger H., Schmidmair D. & Orlova M., 2017. Temperature- and moisture-dependent studies on alunogen and the crystal structure of meta-alunogen determined from laboratory powder diffraction data. *Physics and Chemistry of Minerals*, 44(2), 95–107. <https://doi.org/10.1007/s00269-016-0840-7>.
- Košek F., Culka A., Žáček V., Laufek F., Škoda R. & Jehlička J., 2018. Native alunogen: A Raman spectroscopic study of a well-described specimen. *Journal of Molecular Structure*, 1157, 191–200. <https://doi.org/10.1016/j.molstruc.2017.12.021>.
- Košek F., Culka A., Rousaki A., Vandenabeele P. & Jehlička J., 2022. Raman spectroscopy of anhydrous and hydrated aluminum sulfates: Experience from burning coal heaps. *Journal of Raman Spectroscopy*, 53(11), 1959–1973. <https://doi.org/10.1002/jrs.6420>.
- Kruszewski Ł., 2013. Supergene sulphate minerals from the burning coal mining dumps in the Upper Silesian Coal Basin, South Poland. *International Journal of Coal Geology*, 105, 91–109. <https://doi.org/10.1016/j.coal.2012.12.007>.
- Kruszewski Ł., 2019. Secondary sulphate minerals from Bhanine Valley coals (South Lebanon) – a crystal-chemical and geochemical study. *Geological Quarterly*, 63(1), 65–87. <https://doi.org/10.7306/gq.1450>.
- Leszczyński S., 1981. Piaskowce ciężkowickie jednostki śląskiej w Polskich Karpatach: studium sedymentacji głębokowodnej osadów gruboklastycznych [Ciężkowice Sandstones of the Silesian Unit in the Polish Carpathians: A study of coarse-clastic sedimentation in the deep-water]. *Annales Societatis Geologorum Poloniae*, 51(3–4), 435–502. <https://geojournals.pgi.gov.pl/asgp/article/view/11985/10463>.
- Leszczyński S., Dziadzio P.S. & Nemeč W., 2015. Some current sedimentological controversies in the Polish Carpathian flysch. [in:] Haczewski G. (ed.), *Proceedings of the Guidebook for Field Trips Accompanying 31st IAS Meeting of Sedimentology Held in Kraków, Kraków, Poland, 22–25 June, 2015*, 247–287.
- Locke A.J., Martens W.N. & Frost R.L., 2007. Thermal analysis of halotrichites. *Thermochimica Acta*, 459(1–2), 64–72. <https://doi.org/10.1016/j.tca.2007.04.015>.
- Luo L., Wen H., Zheng R., Liu R., Li Y., Luo X. & You Y., 2019. Subaerial sulfate mineral formation related to acid aerosols at the Zhenzhu Spring, Tengchong, China. *Mineralogical Magazine*, 83(3), 381–392. <https://doi.org/10.1180/mgm.2018.164>.
- Marszałek M., Gawęł A. & Włodek A., 2020. Pickeringite from the Stone Town Nature Reserve in Ciężkowice (the Outer Carpathians, Poland). *Minerals*, 10(2), 187. <https://doi.org/10.3390/min10020187>.
- Martin R., Rodgers K.A. & Browne P.R.L., 1999. The nature and significance of sulphate-rich aluminous efflorescences from the Te Kopia geothermal field, Taupo volcanic Zone, New Zealand. *Mineralogical Magazine*, 63(3), 413–419. <https://doi.org/10.1180/002646199548501>.
- Menchetti S. & Sabelli C., 1974. Alunogen: its structure and twinning. *Tschermaks Mineralogische und Petrographische Mitteilungen*, 21, 164–178. <https://doi.org/10.1007/BF01081029>.
- Munsell Color, 1998. *Munsell Soil Color Charts*. Munsell Color GretagMacbeth. New Windsor, New York.
- Naglik B. & Natkaniec-Nowak L., 2015. Pickeringite from the Pieprzowe Mts. (the Holy Cross Mts., Central Poland). *Geology, Geophysics & Environment*, 41(1), 114–115. <https://doi.org/10.7494/geol.2015.41.1.114>.
- Naglik B., Heflik W. & Natkaniec-Nowak L., 2016a. Charakterystyka mineralogiczno-petrograficzna utworów klastycznych Gór Pieprzowych (Wyżyna Sandomierska) i produktów ich wietrzenia [Mineralogical and petrographic characteristics of clastic rocks of the [!] Mts. (Sandomierz Upland) and their weathering cover]. *Przegląd Geologiczny*, 64(5), 338–343. <https://geojournals.pgi.gov.pl/pg/article/view/27380/19098>.
- Naglik B., Natkaniec-Nowak L. & Heflik W., 2016b. Mineral assemblages as a record of the evolutionary history of the Pepper Mts. Shale Formation (the Holy Cross Mts.). *Geology, Geophysics & Environment*, 42(2), 161–173. <https://doi.org/10.7494/geol.2016.42.2.161>.

- Parafiniuk J., 1996. Sulfate minerals and their origin in the weathering zone of the pyrite-bearing schists at Wieściszowice (Rudawy Janowickie Mts, Western Sudetes). *Acta Geologica Polonica*, 46(3–4), 353–414.
- Parafiniuk J. & Stępisiewicz M., 1999. Sulphate minerals forming of pyrite and marcasite specimens stored under room conditions. *Mineralogia Polonica*, 30(1), 59–71.
- Přikryl R., Melounová L., Vařilová Z. & Weishauptová Z., 2007. Spatial relationships of salt distribution and related physical changes of underlying rocks on naturally weathered sandstone exposures (Bohemian Switzerland National Park, Czech Republic). *Environmental Geology*, 52, 409–420. <https://doi.org/10.1007/s00254-006-0589-2>.
- Quartieri S., Triscari M. & Viani A., 2000. Crystal structure of the hydrated sulphate pickeringite ($\text{MgAl}_2(\text{SO}_4)_4 \cdot 22\text{H}_2\text{O}$): X-ray powder diffraction study. *European Journal of Mineralogy*, 12(6), 1131–1138. <https://doi.org/10.1127/ejm/12/6/1131>.
- Rodríguez A. & van Bergen M.J., 2017. Superficial alteration mineralogy in active volcanic systems: An example of Poás volcano, Costa Rica. *Journal of Volcanology and Geothermal Research*, 346, 54–80. <https://doi.org/10.1016/j.jvolgeores.2017.04.006>.
- Rothman L.S., Gamache R.R., Tipping R.H., Rinsland C.P., Smith M.A.H., Benner D.C., Devi V.M. et al., 1992. The HITRAN molecular database: Editions of 1991 and 1992. *Journal of Quantitative Spectroscopy and Radiative Transfer*, 48, (5–6), 469–507. [https://doi.org/10.1016/0022-4073\(92\)90115-K](https://doi.org/10.1016/0022-4073(92)90115-K).
- Stracher G.B., Prakash A., Schroeder P., McCormack J., Zhang X., Van Dijk P. & Blake D., 2005. New mineral occurrences and mineralization processes: Wuda coal-fire gas vents of Inner Mongolia. *American Mineralogist*, 90(11–12), 1729–1739. <https://doi.org/10.2138/am.2005.1671>.
- Szabo R., Popescu G.C., Dumitraș D.-G. & Ghinescu E., 2020. New occurrences of sulfate minerals in Jiul de Vest Upper Basin, South Carpathians, Romania. *Carpathian Journal of Earth and Environmental Sciences*, 15(2), 347–358. <https://doi.org/10.26471/cjees/2020/015/135>.
- Vařilová Z., Přikryl R. & Cílek V., 2011. Pravčice Rock Arch (Bohemian Switzerland National Park, Czech Republic) deterioration due to natural and anthropogenic weathering. *Environmental Earth Science*, 63(7–8), 1861–1878. <https://doi.org/10.1007/s12665-010-0881-z>.
- Wang A. & Zhou Y., 2014. Experimental comparison of the pathways and rates of the dehydration of Al-, Fe-, Mg- and Ca-sulfates under Mars relevant conditions. *Icarus*, 234, 162–173. <https://doi.org/10.1016/j.icarus.2014.02.003>.
- Wieser T., 1949. Siarczane produkty wietrzenia na złożu dwusiarczku żelaza Gór Świętokrzyskich. *Annales Societatis Geologorum Poloniae*, 19(3), 445–477.
- Williams R.B.G. & Robinson D.A., 1998. Weathering of sandstone by alunogen and alum salts. *Quarterly Journal of Engineering Geology*, 31(4), 369–373. <https://doi.org/10.1144/GSL.QJEG.1998.031.P4.10>.
- Žáček V., 1988. Zonal association of secondary minerals from burning dumps of coal mines near Kladno, Central Bohemia, Czechoslovakia. *Acta Universitatis Carolinae, Geologica*, 3, 315–341.
- Žáček V. & Skála R., 2015. Mineralogy of burning-coal waste piles in collieries of the Czech Republic. [in:] Stracher G.B., Sokol E.V. & Prakash A. (eds.), *Coal and Peat Fires: A Global Perspective, Volume 3: Case Studies – Coal Fires*, Elsevier, Amsterdam, Boston, Heidelberg, London, 109–160.